Supporting Information

Structural Disorder and Spin Dynamics Study in Millimeter Size All-Inorganic Lead Free Cesium Bismuth Halide Perovskite Single Crystals

Naveen Kumar Tailor, [1] Soumitra Satapathi, [1,*]

[1] Department of Physics, Indian Institute of Technology Roorkee, Roorkee, Haridwar, 247667, Uttarakhand, India

*Corresponding Author: ssphf.fph@iitr.ac.in

1. Materials and Methods

1.1. Materials

Cesium chloride (CsCl) (99%) and bismuth chloride ($BiCl_3$) (98%) was purchased from Avra Synthesis Pvt. Ltd. Cesium Bromide (CsBr) (99.9% trace metal basis) and bismuth bromide ($BiBr_3$) (>98%) was purchased from Sigma Aldrich. Cesium iodide (CsI) (>99.0%) and bismuth iodide anhydrous (BiI3) (>98.0%) was purchased from the TCI chemicals. Hydrochloric acid (HCl 35-38%) was purchased from s d fine-CHEM limited (SDFCL). Hydrobromic acid (HBr, 48-49% in water) was purchased from Sisco research laboratories Pvt. Ltd. (SRL). GBL (γ-Butyrolactone) extrapure was purchased from SRL. Deionized (DI) water was also used as a solvent. All chemicals were used as received without further purification.

1.2. Synthesis of $Cs_3Bi_2Cl_9$ SC

Synthesis of the $Cs_3Bi_2Cl_9$ single crystals was carried out by a slow cooling method. Cesium chloride solution was prepared in DI water. 3 mol of cesium chloride is dissolved in 10 ml of DI water under continuous magnetic stirring at 120 ^oC until no powder is observed. 2 mol of bismuth chloride is dissolved in 8 ml DI water and 2 ml HCl solution is prepared under continuous magnetic stirring at 120 ^oC until a homogeneous solution is formed. For the synthesis of $Cs_3Bi_2Cl_9$ crystals, cesium chloride and bismuth chloride solution were mixed in a well-cleaned glass vial and stirred at 120 ^oC. The reaction in the synthesis of $Cs_3Bi_2Cl_9$ can be written using the following Equation 1.

$$3CsCl + 2BiCl_3 \longrightarrow Cs_3Bi_2Cl_9 \quad (1)$$

We used the slow cooling method for growing $Cs_3Bi_2Br_9$ perovskite single crystal. In this method, the precursor solution was cooled from 120 ^oC to room temperature with a cooling rate of 0.3 ^oC per 1 hour. There was no seed placed in solution so homogeneous nucleation occurs and single crystals grew in this process. The nucleation rate and the crystal growth process depends on controlling the temperature cooling rate. After reach to the room temperature solution was left in ambient condition for a few days.

1.3. Synthesis of $Cs_3Bi_2Br_9$ SC

Synthesis of the $Cs_3Bi_2Br_9$ single crystals was also carried out by a slow cooling method. Cesium Bromide solution was prepared in DI water. 3 mol of cesium bromide dissolved in 10 ml DI water under continuous magnetic stirring at 120˚ C until no powder is observed. 2 mol of bismuth bromide dissolved in 10 ml HBr and solution is prepared under continuous magnetic stirring at 120˚C until formed homogeneous solution. For the synthesis of $Cs_3Bi_2Br_9$ crystals, cesium bromide and bismuth bromide solution were mixed in a well-cleaned glass vial and stirred at 120^oC. The reaction in the synthesis of $Cs_3Bi_2Br_9$ can be written using the following equation 2.

$$3CsBr + 2BiBr_3 \longrightarrow Cs_3Bi_2Br_9 \quad (2)$$

The solution was heated at 120 ^oC for 1 hour. Then the solution was cooled from 120 ^oC to room temperature with a cooling rate of 0.3 ^oC per 1 hour. After reach to the room temperature solution was left in ambient condition for a few days.

1.4. Synthesis of $Cs_3Bi_2I_9$ SC

Synthesis of the $Cs_3Bi_2I_9$ single crystals was carried out by Inverse Temperature Crystallization (ITC) method. According to the stoichiometric ratio of $Cs_3Bi_2I_9$, 3 mol CsI and 2 mol BiI_3 were dissolved into 5 ml GBL under continuous magnetic stirring at 60˚ C until no powder is observed. During the dissolving process, the color of the mixed solution gradually turned crimson. Finally, the dark crimson transparent solution was obtained as the precursor. Now the temperature was increased up to 120 ^oC with a heating rate of 0.5 ^oC per hour. At 120 ^oC we put the solution for two days. After two days, we obtained millimeter sizes Cs3Bi2I9 single crystals. There was no seed placed in solution so homogeneous nucleation occurs and single crystals grew in this process. The reaction in the synthesis of $Cs_3Bi_2I_9$ can be written using the following equation 3.

$$3CsI + 2BiI_3 \longrightarrow Cs_3Bi_2I_9 \quad (3)$$

2. Characterizations

2.1. Morphology

Photographs of crystals were taken using a DSLR camera. Surface images were taken using Field emission scanning electron microscope (FESEM) model FESEM QUANTA 200 FEG under electron excitation energy of 20 keV using ETD detector at 1000 magnification. Surface roughness was measured using the atomic force microscopy model NT-MDT-INTEGRA.

2.2. X-ray diffraction measurement

Powder x-ray diffraction data-sets of all lead-free single crystal were collected using a Bruker (D8-Advance Model) diffractometer equipped with a LINXEYE XE detector using Cu-Kα radiation (λ = 1.54 Å).

2.3. Optical measurements

Ultraviolet-visible (UV-vis) absorption spectra of single-crystal were collected using a Microprocessor UV-Vis Double Beam spectrophotometer LI-2800. Photoluminescence measurements were performed with an RF-6000 Spectro-Fluorophotometer. For the Raman spectra measurement, the WITec alpha300 RA Raman instrument was used with the laser source 532 nm.

2.4. ESR measurement

ESR spectra of all single crystals were measured BY BRUKER BIOSPIN, Germany Model-EMXmicro A200-9.5/12/S/W Microwave X Band source. The magnetic field was applied in the range of 1000 Gauss to 6000 Gauss. The microwave frequency of 9.4 GHz was used. We obtained the first derivative of the absorptive ESR signal. The g value is calculated using the relation

$$h\upsilon = g\mu_B B \quad (4)$$

where h is Planck's constant, υ is the microwave frequency, μ_B is the Bohr magneton, and B is applied magnetic field.

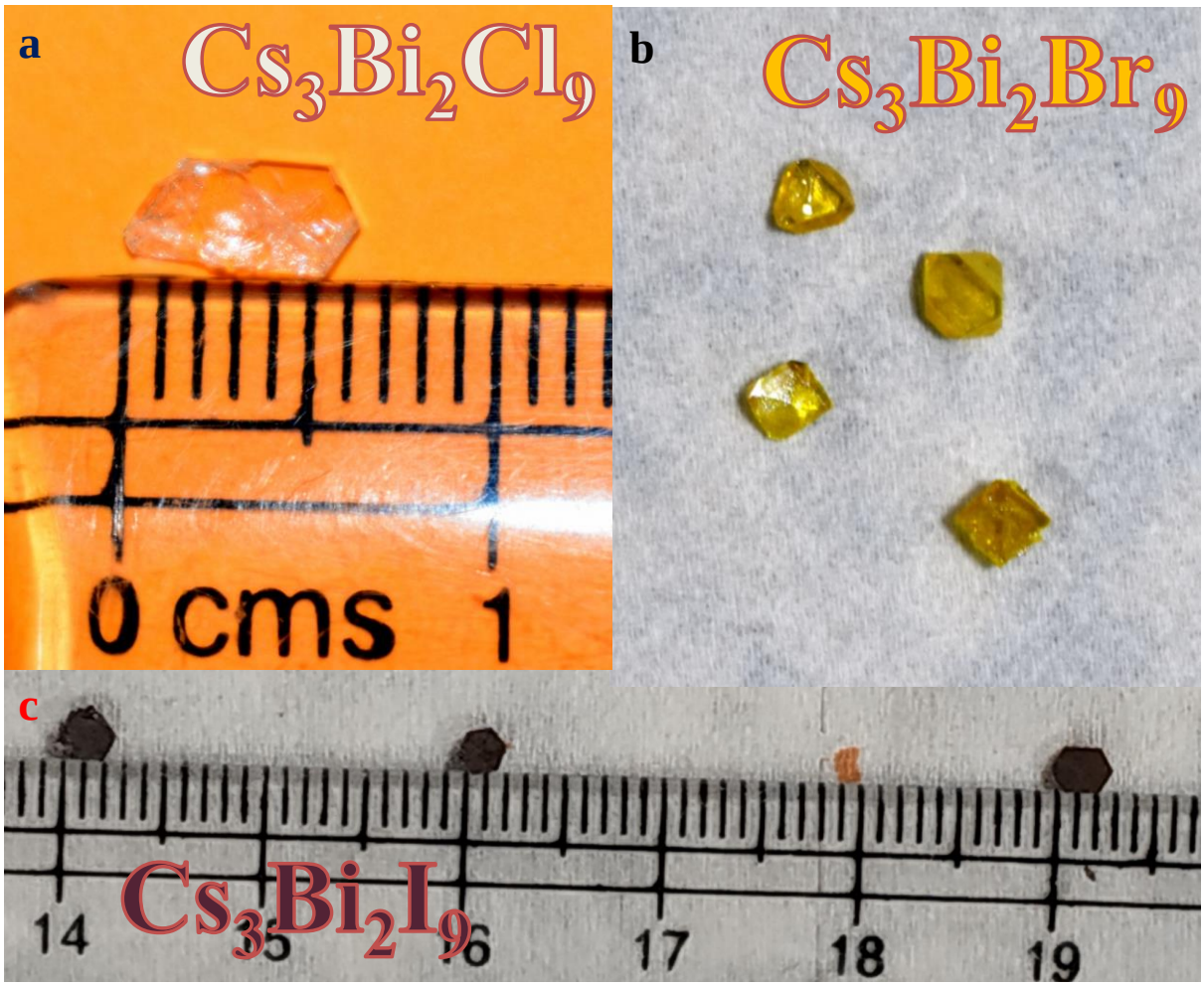

Figure S1. Photographs of the as grown lead free perovskite single crystals. (a) $Cs_3Bi_2Cl_9$ single crystals (b) $Cs_3Bi_2Br_9$ single crystal and (c) $Cs_3Bi_2I_9$ single crystal.

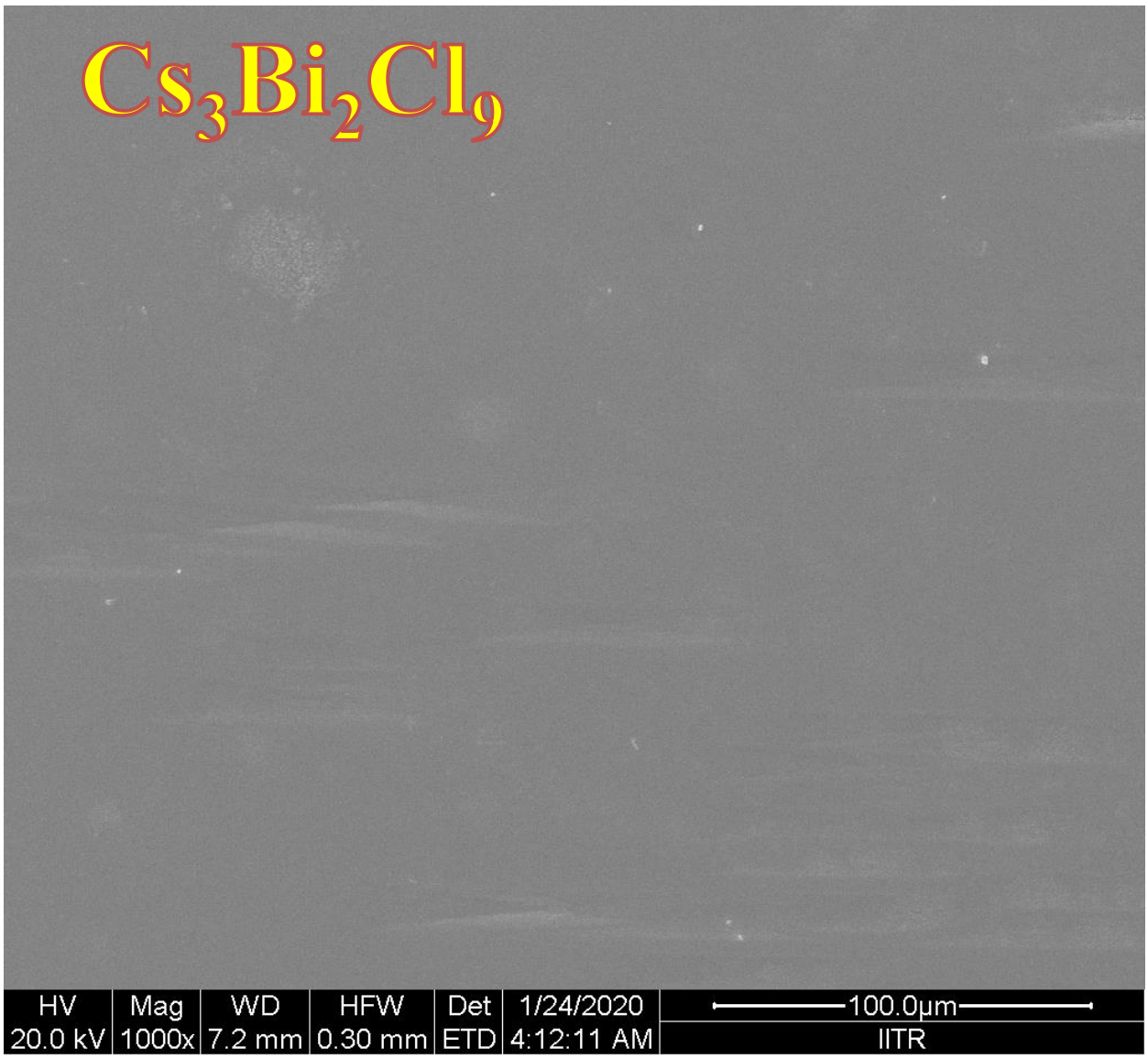

Figure S2. Surface morphology image of $Cs_3Bi_2Cl_9$ single crystal.

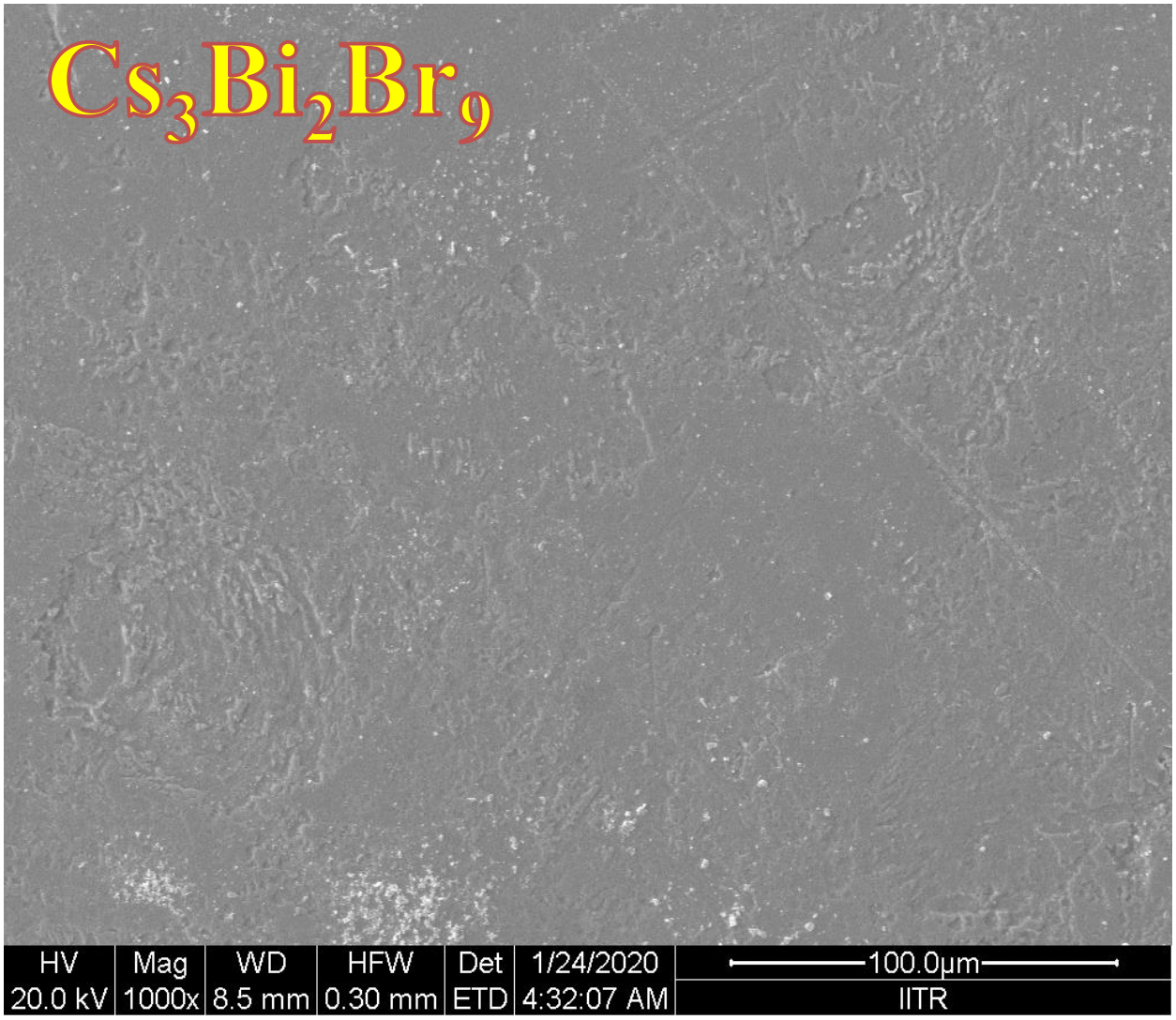

Figure S3. Surface morphology image of $Cs_3Bi_2Br_9$ single crystal.

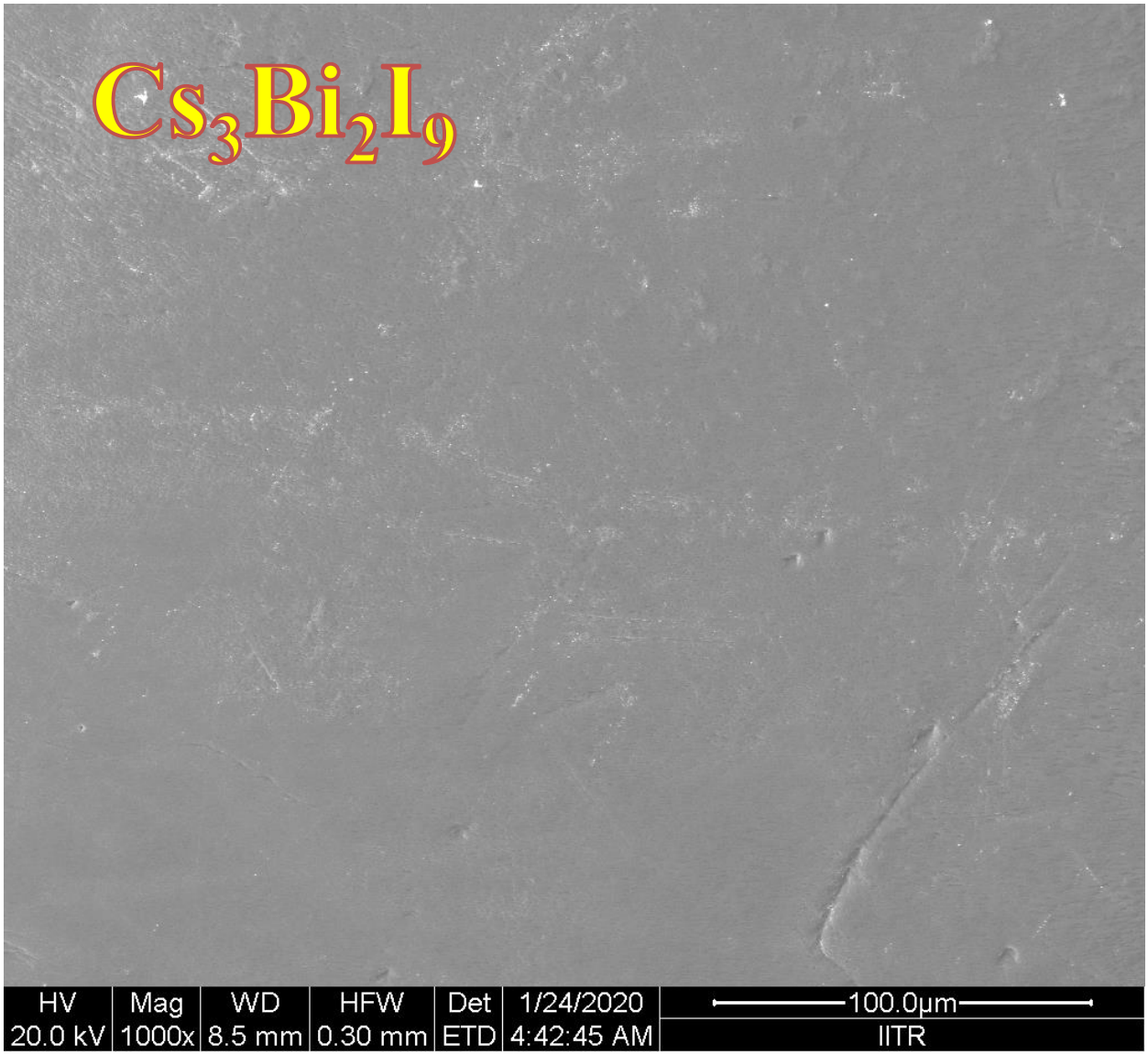

Figure S4. Surface morphology image of $Cs_3Bi_2I_9$ single crystal.

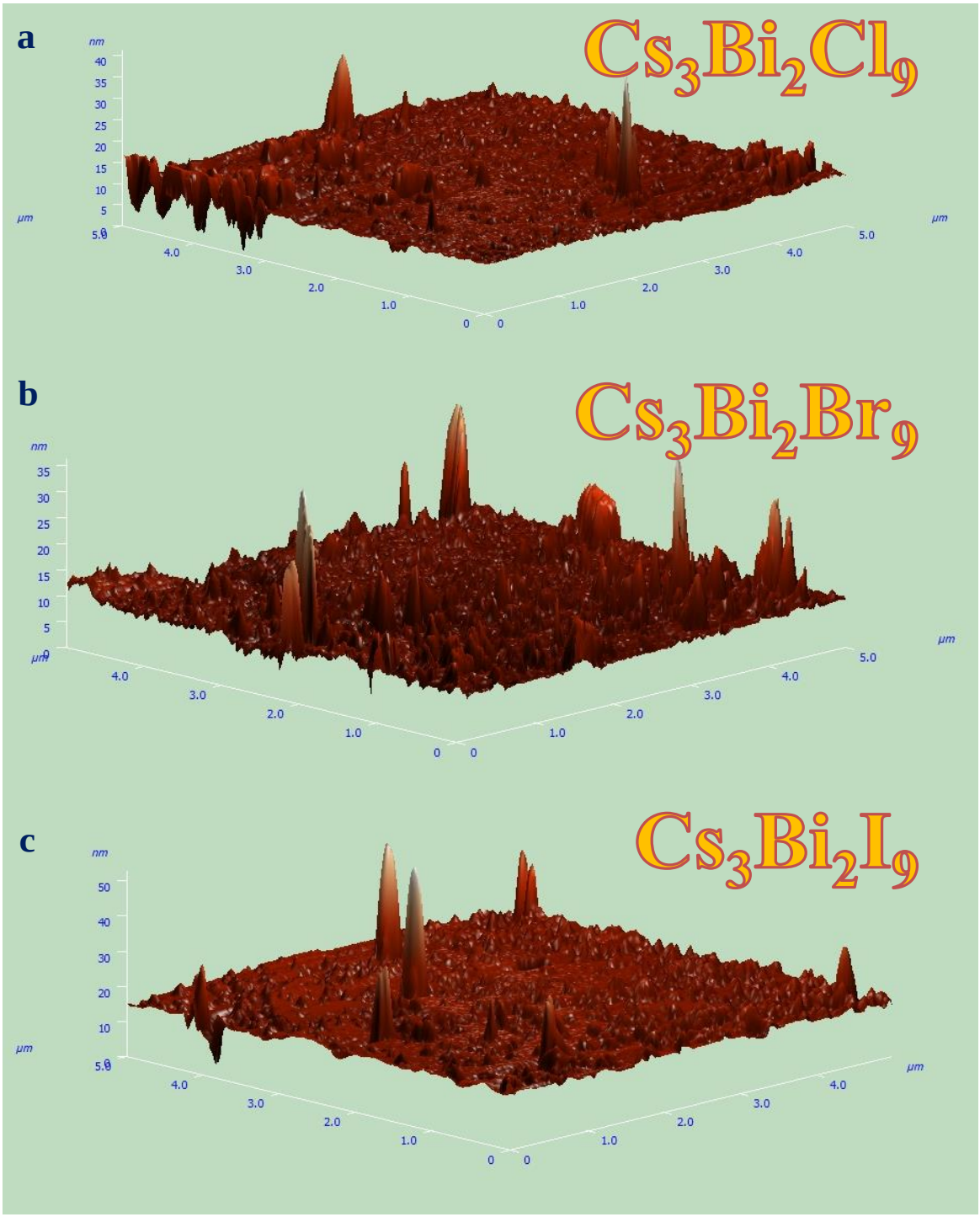

Figure S5. 3D view of surface roughness image of lead-free perovskite single crystals. (a) $Cs_3Bi_2Cl_9$ single crystals (b) $Cs_3Bi_2Br_9$ single crystal and (c) $Cs_3Bi_2I_9$ single crystal.

3. Bandgap calculation

The absorption coefficient is given by the following equation:

$$\alpha = \frac{A(h\upsilon - E_g)^m}{h\upsilon} \quad (5)$$

$$(\alpha h\upsilon)^{\frac{1}{m}} = A^{\frac{1}{m}} h\upsilon - A^{\frac{1}{m}} E_g \quad (6)$$

where A is absorbance, hυ is the photon energy represented in eV units 1240/(incident wavelength in nm). If you plot a graph of $(\alpha h\upsilon)^{1/m}$ against hυ, then the hυ axis intercept $(\alpha h\upsilon)^{1/m} = 0$ of the linear slope fitted to the linear section of the plot will give the bandgap Eg. Wherein: m = ½ for direct bandgap semiconductors, m = 2 for indirect bandgap semiconductors, m = 3 for semiconductors with direct forbidden transitions, and m = 4 for semiconductors with indirect forbidden transitions.

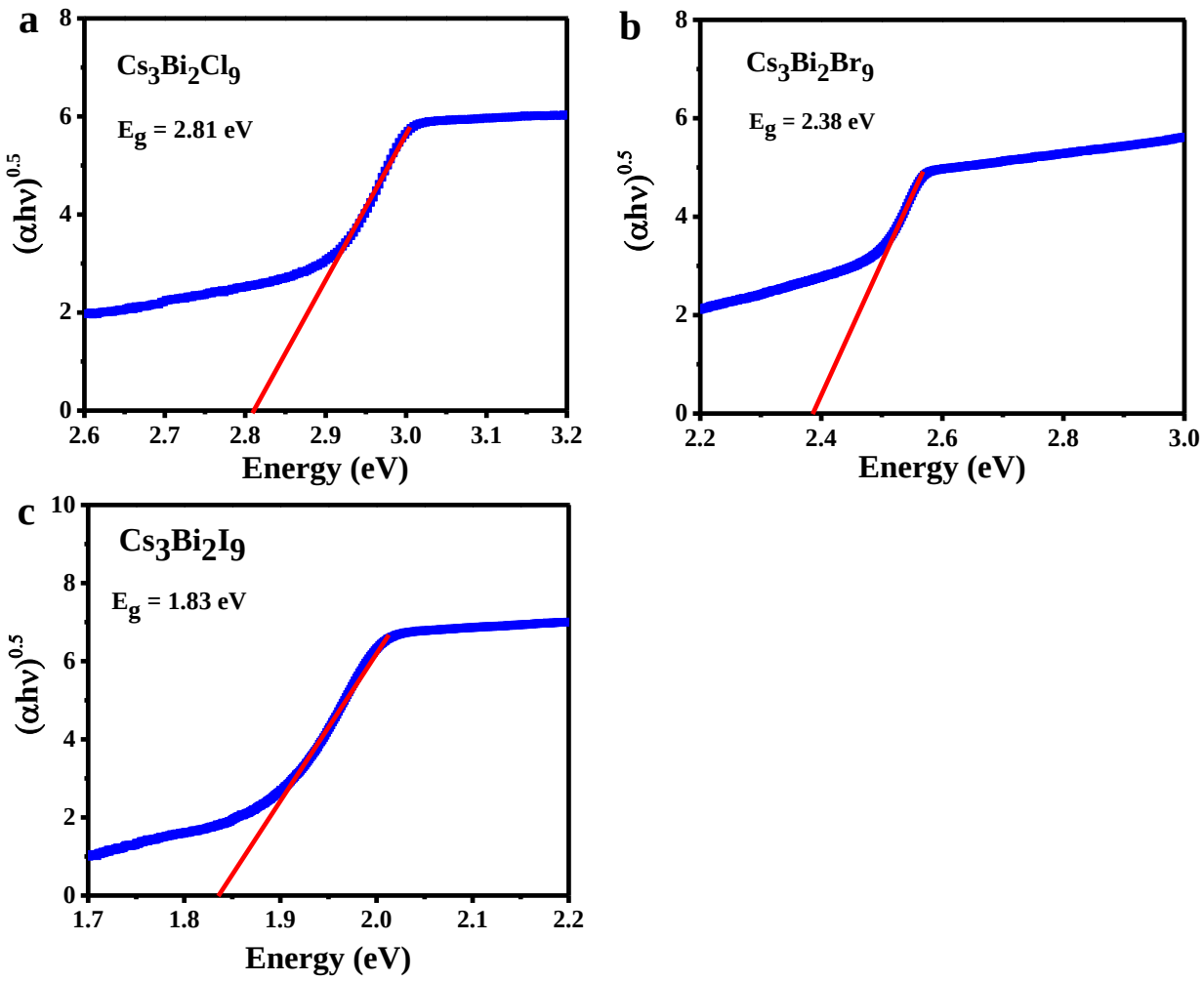

Figure S6. Tauc plots of lead free perovskite single crystals for the calculation of indirect bandgap. (a) $Cs_3Bi_2Cl_9$ single crystals (2.81 eV) (b) $Cs_3Bi_2Br_9$ single crystal (2.38 eV) and (c) $Cs_3Bi_2I_9$ single crystal (1.83 eV).

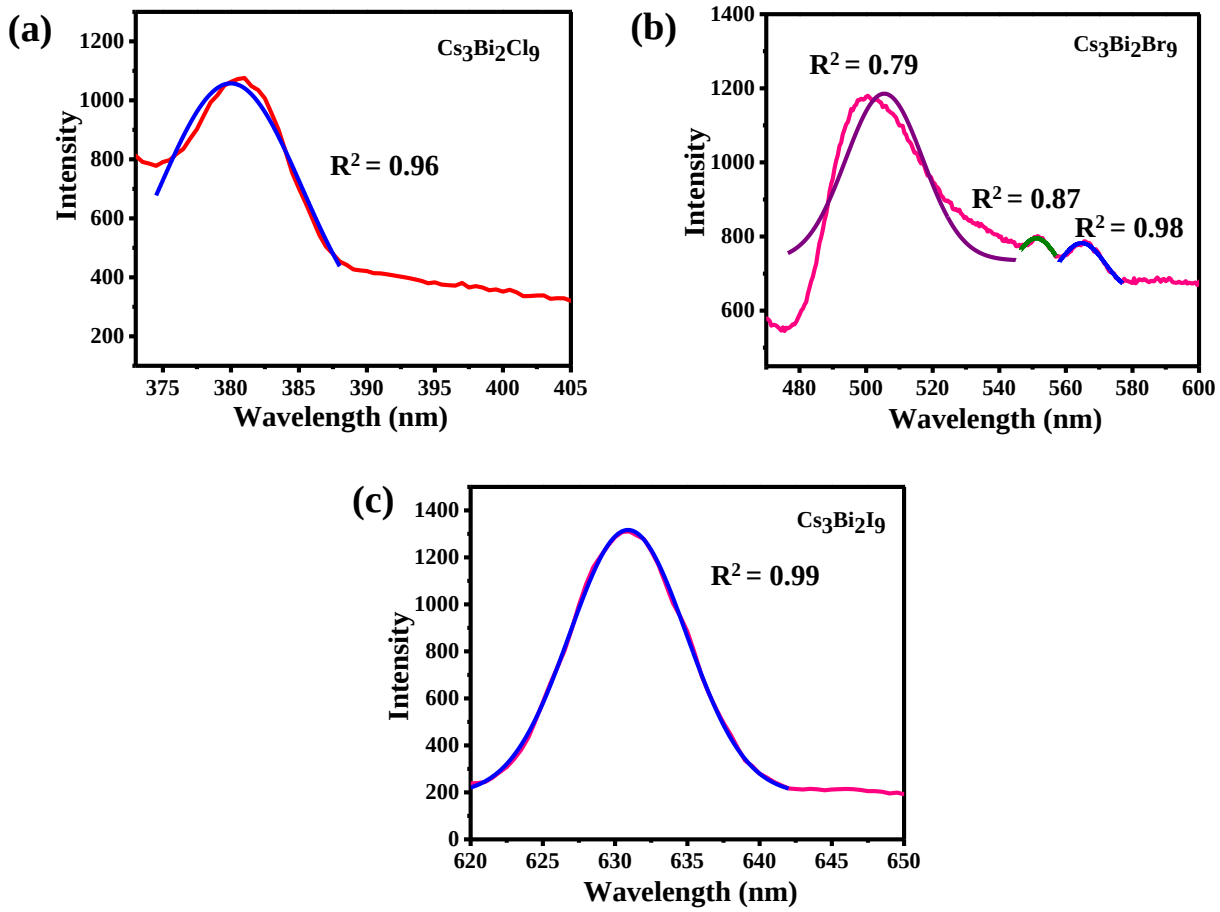

Figure S7. The Gaussian fitting of the PL peaks. (a) $Cs_3Bi_2Cl_9$ single crystal (b) $Cs_3Bi_2Br_9$ single crystal and (c) $Cs_3Bi_2I_9$ single crystal.

4. Raman Spectra Analysis

For the investigation of information about structural features of crystals and the role of Bi-X bonds in optical properties of the crystals, we measured the Raman spectra of all crystal using a 532 nm excitation source. In the $Cs_3Bi_2Cl_9$ SC, we observed the Raman peaks at 78, 115, 243, 265, and 294 cm^{-1} as shown in Figure S8(a). The three bands at 243, 265, and 294 cm^{-1} are due to the Bi-Cl bond vibration in $[Bi_2Cl_9]^{3-}$.[1] The peaks in the lower frequency region at 78, 115 cm^{-1} are due to the movement of Cl atoms without any participation of the Bi atom. $BiCl_3$ gives symmetric and asymmetric stretching bands at 294 and 265 cm^{-1}, respectively, with bending activity at 115 cm^{-1}. In CBBr crystal, raman peaks arises at 77, 175 and 201 cm^{-1}(Figure S8(b)). The CBBr single crystal exhibit trigonal system with space group D_{3d}^3 & P-3ml, therefore nine fundamental Raman active modes can be expected. In CBBr crystal structure, there are two groups of Br atoms. In the first group, there are six ($Br^{(2)}$) atoms with C_S site symmetry, which are included in $BiBr_6$ octahedra. Three atoms ($Br^{(1)}$) are located in position C_{2h} and belong to bridges connecting the neighboring octahedra. In $BiBr_6$ octahedra, the vibrations of Bi-Br bonds causes the Raman bands. Two vibrations are related with bands (175 cm^{-1} and 202 cm^{-l}) in CBBr. The remaining vibrations connected with $BiBr_6$ octahedra are due to the movement of $Br^{(2)}$ atoms only (without the participation of Bi) and they may generate the low-frequency bands.[1-4]

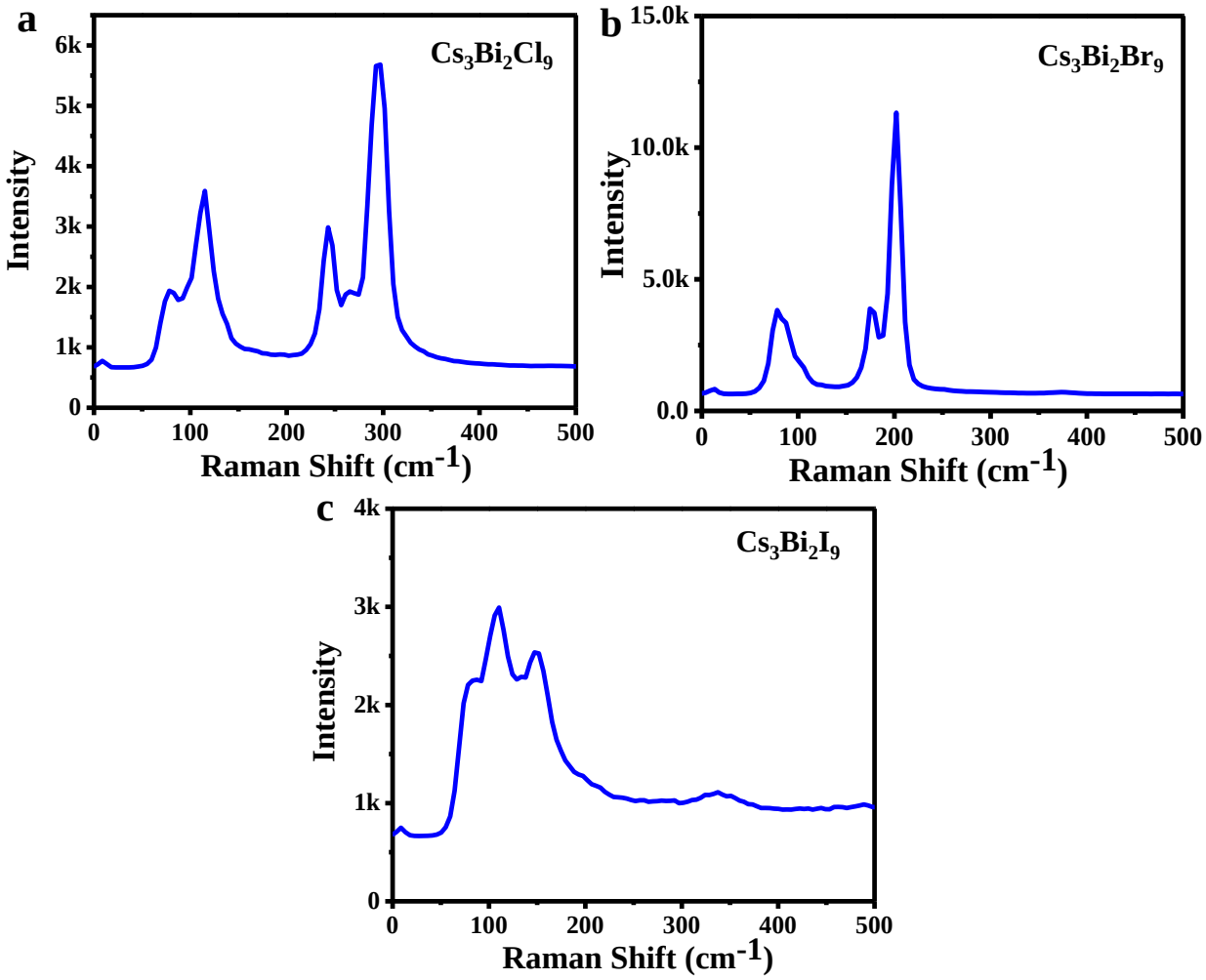

Figure S8. Raman spectra of (a) CBCl crystal, (b) CBBr crystal, and (c) CBI crystal. The excitation wavelength is used as 532 nm.

In the CBI SC, the Raman peaks occur at 85, 108, 132, 147 cm^{-1} (Figure S8(c)). The crystal structure of CBI consists of molecular $[Bi_2I_9]^{3-}$ anions bound together by three Cs^+ cations per unit. In this crystal, the dominant vibrations occur due to strongly bound $[Bi_2I_9]^{3-}$ unit and weaker vibrations from the ionic interactions of $[Bi_2I_9]^{3-}$ unit with the bridging Cs^+ cations. The major vibrational modes in the $[Bi_2I_9]^{3-}$ unit are the Bi-I stretching modes associated with the six terminal I atoms and the three bridging I atoms that connect the two Bi atoms together. The bridging iodine atoms share their bonds with two Bi atoms so the force constants for bridging Bi−I bonds are weaker than the terminal Bi−I bonds. Therefore, the peaks at high energy are attributed to the stretching modes of the terminal bonds. The peak at 147 cm^{-1} and 132 cm^{-1} is assigned to the symmetric and asymmetric terminal Bi-I stretch respectively. The peak at 108 cm^{-1} and 85 cm^{-1} is assigned to the bridge Bi-I symmetric and asymmetric stretch respectively. We are not able to

observe weaker modes at the low-frequency regime, which indicates the less ionic interaction between Cs^+ and $[Bi_2I_9]^{3-}$ unit.[5]

5. ESR Spectroscopy

In the ESR there are two relaxation processes occur. First is the spin-lattice or longitudinal relaxation time T_1, which describes the spins 'dropping' from the upper energy level to the lower level with excess energy dissipated through thermal vibrations of the lattice. The ESR spectrum line width is altered by the T_1 because it relates to the upper energy level lifetime. According to Heisenberg's uncertainty principle, a large T_1 leads to sharper lines, and vice versa. Second is the spin-spin or transverse relaxation time T_2, which describes the redistribution of energy within an ensemble of spins and occurs with no net energy change. T_2 affects the linewidth through spin-spin dipolar and exchange interactions. The relation between T_1 and T_2 is given by the following equation:[6]

$$Half\ Width\ \Delta B = \frac{1}{T_m} = \frac{1}{T_2} + \frac{1}{2T_1} \qquad (7)$$

6. Thermal Stability

To investigate the thermal stability of lead-free SCs, we measure the thermal gravetic analysis (TGA) and differential temperature analysis (DTA), and results are display in Figure S9. We observe that CBI SCs are stable up to 280 ^{o}C, CBBr SCs are stable up to 260 ^{o}C and CBCl SCs are stable up to 220 ^{o}C. These results suggest that CBI has higher thermal stability. We also perform the TG measurements of the precursor materials CsX and BiX_3 and find that the component CsX (X= Cl, Br, I) undergo weight loss in a single step, with the almost same onset temperature at 630 ^{o}C and component BiX_3 (X= Cl, Br, I) undergo weight loss in a single step, with the onset temperature at 200 ^{o}C, 230 ^{o}C and 280 ^{o}C respectively which suggest clear sublimation without complex decomposition for this lead-free perovskite. We find that $Cs_3Bi_2X_9$ decomposes in multiple steps, and all CsX and BiX_3 are sublimed in a single mass-loss step at a well-defined temperature, which suggests that these species are incorporated into the perovskite structure. One interesting observation is that CsX undergoes weight loss with onset temperature at 630 ^{o}C while in organic species like CH_3NH_3X (X= Cl, Br, I) undergo weight loss with the onset temperature at 171 ^{o}C, 202 ^{o}C, and 202 ^{o}C respectively, suggesting that Cs-based material are more thermally stable.[7] Differential thermal analysis reveals the exothermic reaction in all crystals as shown in Figure S9 (d).

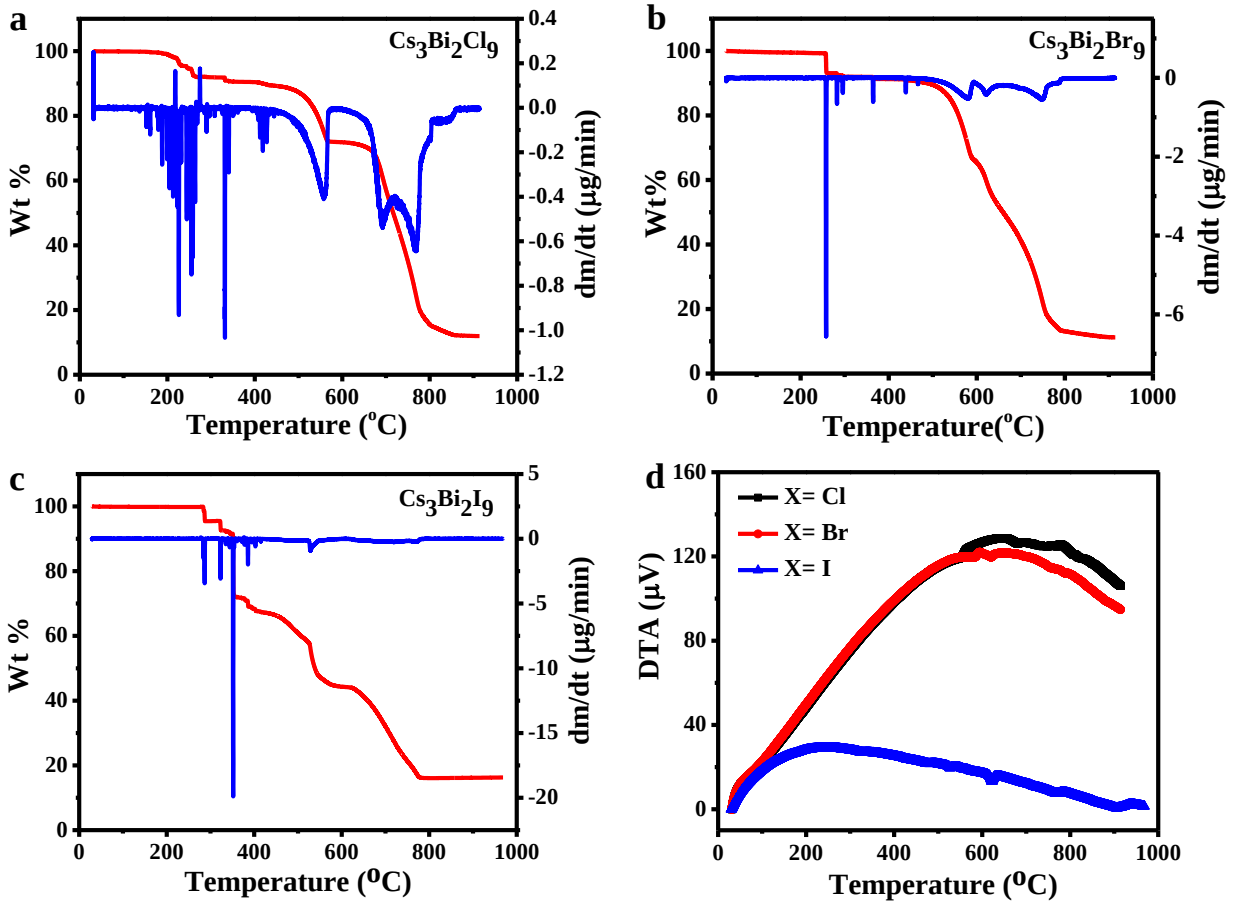

Figure S9. The thermal stability analysis of the lead free perovskite single crystals. (a-c) TGA and derivative of TG curves of $Cs_3Bi_2X_9$ (X = Cl, Br, I) respectively. (d) DTA curves of $Cs_3Bi_2X_9$ (X = Cl, Br, I) respectively.

References

(1) Plane, R. P. O. a. R. A., Raman spectra of solid bismuth(III) bromide and chloride. *Inorg. Chem.* **1969,** 8.
(2) Pistor, P.; Meyns, M.; Guc, M.; Wang, H.-C.; Marques, M. A. L.; Alcobé, X.; Cabot, A.; Izquierdo-Roca, V., Advanced Raman spectroscopy of Cs2AgBiBr6 double perovskites and identification of Cs3Bi2Br9 secondary phases. *Scripta Materialia* **2020,** 184, 24-29.
(3) Kentsch, R.; Scholz, M.; Horn, J.; Schlettwein, D.; Oum, K.; Lenzer, T., Exciton Dynamics and Electron–Phonon Coupling Affect the Photovoltaic Performance of the Cs2AgBiBr6 Double Perovskite. *J. Phys. Chem. C* **2018,** 122, (45), 25940-25947.
(4) Valakh, M. Y.; Lisitsa, M. P.; Peresh, E. Y.; Trylis, O. V.; Yaremko, A. M., The Raman spectra of the family crystals Cs3Bi2Br9, Rb3Bi2Br9 and Rb3Sb2Br9. *J. Mol. Struct.* **1997,** 437, 309-313.
(5) McCall, K. M.; Stoumpos, C. C.; Kostina, S. S.; Kanatzidis, M. G.; Wessels, B. W., Strong Electron–Phonon Coupling and Self-Trapped Excitons in the Defect Halide Perovskites A3M2I9 (A = Cs, Rb; M = Bi, Sb). *Chem. Mater.* **2017,** 29, (9), 4129-4145.
(6) Roessler, M. M.; Salvadori, E., Principles and applications of EPR spectroscopy in the chemical sciences. *Chem. Soc. Rev.* **2018,** 47, (8), 2534-2553.
(7) Liu, Y.; Yang, Z.; Cui, D.; Ren, X.; Sun, J.; Liu, X.; Zhang, J.; Wei, Q.; Fan, H.; Yu, F.; Zhang, X.; Zhao, C.; Liu, S. F., Two-Inch-Sized Perovskite CH3 NH3 PbX3 (X = Cl, Br, I) Crystals: Growth and Characterization. *Adv. Mater.* **2015,** 27, (35), 5176-83.